Anomalous Screening Effect of Superlattice-Doped GaAs/(Al,Ga)As Heterostructures under Illumination

Xiao-Fei Liu[1,*] Nikolai Spitzer[2] Haruki Kiyama[1,3] Arne Ludwig[2] Andreas D. Wieck[2] and Akira Oiwa[1,4,5,6]

[1]*SANKEN, Osaka University, 8-1 Mihogaoka, Ibaraki, Osaka 567-0047, Japan*

[2]*Lehrstuhl für Angewandte Festkörperphysik, Ruhr-Universität Bochum, Universitätsstraße 150, Gebäude NB, Bochum D-44780, Germany*

[3]*Graduate School of Information Science and Electrical Engineering, Kyushu University, Fukuoka 819-0395, Japan*

[4]*Center for Quantum Information and Quantum Biology (QIQB), Osaka University, Osaka 565-0871, Japan*

[5]*Center for Spintronics Research Network (CSRN), Graduate School of Engineering Science, Osaka University, Osaka 560-8531, Japan*

[6]*Spintronics Research Network Division, OTRI, Osaka University, Osaka 565-0871, Japan*

The GaAs/(Al,Ga)As heterostructure with short-period superlattice (SPSL) doping possesses ultrahigh mobility of its two-dimensional electron gas by placing donors within the remote GaAs layers. Here, we investigate its magnetotransport property under a heavily doped situation. After long enough illumination at cryogenic temperature, the change of the electron concentration inside the quantum well (QW) is only 5.9%. Meanwhile, the quantum lifetime $\tau_{q,\text{QW}}$ of the electron shows an anomalous behavior. It increases slightly and then exhibits an exponential decay until saturation. This is different from the monotonic increase of $\tau_{q,\text{QW}}$ under illumination for the conventional doping situation. The increase of $\tau_{q,\text{QW}}$ originates from the larger donor filling-fraction-enhanced screening effect. Meanwhile, the decrease of $\tau_{q,\text{QW}}$ may be caused by stronger scattering of ionized d^+ states evolved from DX centers. The transfer of excess electrons between the AlAs layers can also cause the decrease of $\tau_{q,\text{QW}}$. This work provides an insight into the mechanism of DX centers on the quantum transport properties of SPSL-doped heterostructures.

I. INTRODUCTION

The high-mobility two-dimensional electron gas (2DEG) system leads to many discoveries in the field of quantum transport and mesoscopic physics [1,2]. The mobility of 2DEG in the GaAs/(Al,Ga)As heterostructure, which is grown by molecular-beam epitaxy (MBE) can be as high as 10^7 cm^2 V^{-1} s^{-1} and exceeds any other two-dimensional (2D), bulk, or heterostructure materials [3]. Generally, conventional GaAs/(Al,Ga)As heterostructure uses modulation or δ doping [4,5]. The interstitial impurities induced and negatively charged deep-donor levels (DX centers [6]) with the energy below the Γ band of (Al,Ga)As can form easily if the AlAs fraction exceeds 22%. The DX centers reduce the efficiency of charge transfer from donors (e.g., Si) to the 2DEG. Of note, the persistent photoconductivity will change the mobility and concentration of the 2DEG (as well as parallel conduction channels) greatly. This strongly disturbs the precise controls and measurements of quantum behaviors in quantum devices formed in GaAs/(Al,Ga)As heterostructures under light illuminations. In order to reduce the formation of DX centers, the undoped heterostructure with top gate shows good performance [7]. Another method is to separate Si donors from AlAs containing layers [8]. The wafer can be grown through δ doping into the GaAs layer of an AlAs/GaAs SPSL, in which the localized electrons can effectively screen potential fluctuations caused by remote ionized impurities [9–13]. Using gate control, the relationship between the mobility and the density of excess electrons has been well investigated in experiment [11]. However, the magnetotransport properties of the SPSL-doped GaAs/(Al,Ga)As heterostructures under illuminations are still unclear up to now.

II. DEVICE FABRICATION

Here, we investigate the effect of illumination on the SPSL-doped GaAs/(Al,Ga)As heterostructure under a heavily doped situation. After removing the
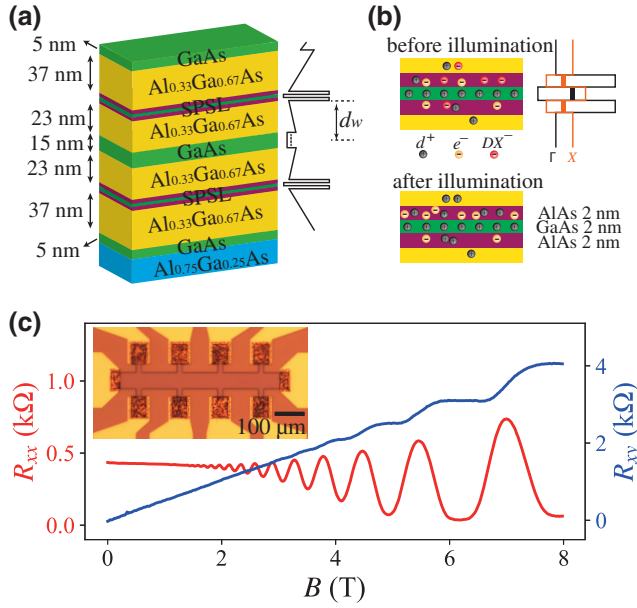
_____

*xfeiliu@163.com

FIG. 1. (a) Layer structure and the corresponding Γ-band energy. (b) Changes of *DX* centers and excess electrons before and after LED illumination. In the SPSL, the GaAs layer is surrounded by two AlAs layers. Donors (Si) are δ doped into this GaAs layer. (c) The transport behavior of this heavily doped wafer measured in ^{3}He fridge with base temperature 0.36 K. Insert is the microscopic picture of the Hall bar.

magnetotransport contributions from parallel conduction channels, the changes of the 2DEG concentration, mobility, and quantum lifetime as functions of light-emitting diode (LED) illumination time are analyzed. The sample used in this experiment is grown by MBE. The buffer layer consists of 104-nm superlattice (2.6 nm/2.6 nm AlAs/GaAs), 50 nm GaAs, and 700 nm $Al_{0.75}Ga_{0.25}As$ on a GaAs substrate. The layer structure above the buffer layer is symmetric, as shown in Fig. 1(a). This heterostructure consists of a 2DEG residing in a 15-nm-wide GaAs QW with depth 71 nm beneath the surface. The electrons of this heterostructure are provided by two δ-doped AlAs/GaAs/AlAs (2 nm/2 nm/2 nm) SPSLs, which are separated by two 23-nm-wide $Al_{0.33}Ga_{0.67}As$ barrier layers from the QW. The donor (Si) concentration n_{Si} in each SPSL is about 2.0×10^{14} cm^{-2}. These two SPSLs are covered by 37-nm undoped $Al_{0.33}Ga_{0.67}As$ layers and 5-nm capping layers. Since the electron ground state of the *X* band in AlAs is lower than that of the quantum confined Γ-band state in GaAs, excess electrons mainly reside in the AlAs layer. This heterostructure is heavily doped and contains a sacrificial layer. When this sacrificial layer is removed to form a suspended structure, the carrier density will decrease together with higher mobility. Furthermore, lateral quantum dots fabricated on this suspended structure can be combined with photonic nanocavities to enhance quantum state conversion from photon polarization to electron spin [14–18].

The measured Hall bar with 650 μm length and 60 μm width is fabricated by photolithography and then etching to a depth of 110 nm from the surface, as shown in the insert of Fig. 1(c). The Ohmic contacts are formed by thermal evaporation of AuGe/Ni (200 nm/20 nm) alloys in high vacuum and then annealing at 420°C for 2 min in the N_2-H_2 (97%–3%) forming gas. An LED with a center wavelength of 860 nm is mounted 1.0 cm above the sample and driven with the current of 125 μA. The magnetotransport of this Hall bar before illumination (measured at 0.36 K) is demonstrated in Fig. 1(c). The sheet carrier density deduced from Shubnikov-de Haas (SdH) oscillation is $n_{SdH} = 1.17 \times 10^{12}$ cm^{-2}, which corresponds to the heavily doped situation. The difference of n_{SdH} and n_{Hall} (measured from the low-field Hall resistance R_{xy}) is about 2.5%, meaning the transport contribution from the SPSLs is small. Figure 1(b) shows the distribution of *DX* centers. Due to the diffusion of Si atoms during MBE growth, most of the *DX* centers are located in the AlAs layers of the SPSLs, while others exist in the $Al_{0.33}Ga_{0.67}As$ barrier layers.

III. ANALYSES OF PARALLEL CONDUCTION

Since the electron mass at the *X* band of the AlAs layer is heavier than that at the Γ band of the GaAs layer [8,19–21], the electric conductivity of the SPSL is small. However, the density of the electrons residing in the AlAs layers of the SPSLs may increase greatly after illumination, which consequently enhances the transport contributions from the SPSLs. Therefore, the main conduction channel (the QW) and the two parallel conduction channels (the SPSLs, represented by p_u and p_l) should be separated in the analysis of applying illumination. The total conductivity is $\sigma^{tot} = \sum_{i=QW,p_u,p_l} \sigma_i$, in which each conductivity σ_i under an applied magnetic field B can be written as [22–24]

$$\sigma_i = \frac{n_i e \mu_i}{1 + \mu_i^2 B^2} \begin{pmatrix} 1 & -\mu_i B \\ \mu_i B & 1 \end{pmatrix}. \qquad (1)$$

Here, n_i and μ_i represent the sheet carrier density and mobility of each conduction channel, respectively. The two parallel conduction channels are assumed to provide equal contributions to the transports for simplicity (represented by subscript p). Note that the transport contribution of the upper SPSL may be smaller than the lower SPSL because of the surface Fermi pinning. However, this does not affect the main result of this paper. After the inversion of the matrix σ^{tot}, the total longitudinal resistance R_{xx} and the Hall resistance R_{xy} become [22–24]

$$R_{xy}^{tot} = \frac{B \gamma_{QW} \gamma_p \alpha_2}{e \left(\alpha_2^2 B^2 + \alpha_1^2 \right)}, \qquad (2)$$

$$R_{xx}^{\text{tot}} = \frac{\gamma_{\text{QW}}\gamma_p\alpha_1}{e\left(\alpha_2^2 B^2 + \alpha_1^2\right)}. \tag{3}$$

In the above equations, $\alpha_1 = n_{\text{QW}}\mu_{\text{QW}}\gamma_p + n_p\mu_p\gamma_{\text{QW}}$ and $\alpha_2 = n_{\text{QW}}\mu_{\text{QW}}^2\gamma_p + n_p\mu_p^2\gamma_{\text{QW}}$. γ_{QW} and γ_p have the expression as $\gamma_{\text{QW}} = 1 + \mu_{\text{QW}}^2 B^2$ and $\gamma_p = 1 + \mu_p^2 B^2$, respectively. It can be easily seen that $R_{xy}^{\text{QW}} = B/\left(n_{\text{QW}}e\right)$ and $R_0^{\text{QW}} = 1/\left(n_{\text{QW}}e\mu_{\text{QW}}\right)$ are satisfied when n_p or μ_p becomes zero (R_0 stands for R_{xx} at zero magnetic field). This corresponds to the situation of single transport channel.

The scattering strength of the electrons inside the SPSLs is much larger than that of the 2DEG in the QW. Meanwhile, considering the heavier electron mass of the X band of the AlAs layer, the relationship $\mu_p \ll \mu_{\text{QW}}$ is always satisfied. Under this condition, the simplified expressions of R_{xy}^{tot} and longitudinal resistance R_0^{tot} (R_{xx}^{tot} under zero magnetic field) are

$$R_{xy}^{\text{tot},s} = \frac{B}{en_{\text{Hall}}} = \frac{B}{e\left(n_{\text{QW}} + 2n_p\alpha_\mu\right)}, \tag{4}$$

$$R_0^{\text{tot},s} = \frac{1}{n_{\text{QW}}e\mu_{\text{QW}}}\left(1 - \frac{n_p\alpha_\mu}{n_{\text{QW}}}\right). \tag{5}$$

Here, $\alpha_\mu = \mu_p/\mu_{\text{QW}}$ stands for the electron mobility ratio of the SPSL to the QW. Figure 2(a) shows the calculated results of the dependence of magnetic field on the Hall resistance R_{xy}. The green solid line (R_{xy}^{QW}) is obtained without considering parallel conduction channels. The expressions denoted as R_{xy}^{tot} and $R_{xy}^{\text{tot},s}$ are represented by the blue

(a)

(b)

FIG. 2. Simulation results of Hall resistance R_{xy} and longitudinal resistance R_0. (a) R_{xy} under different magnetic field B. (b) R_0 versus different n_p. The parameter values are $\mu_{\text{QW}} = 1.00 \times 10^4$ cm^2 V^{-1} s^{-1}, $\mu_p = 0.05 \times 10^4$ cm^2 V^{-1} s^{-1}, and $n_{\text{QW}} = 1.20 \times 10^{12}$ cm^{-2}. In (a), $n_p = 2.50 \times 10^{12}$ cm^{-2}.

solid line with circle markers and the red dashed line with square markers, respectively. This figure indicates that the simplified expression of $R_{xy}^{\text{tot},s}$ agrees well with R_{xy}^{tot}. Figure 2(b) shows the calculated results of R_0 as a function of n_p. The red dashed line with square symbols (blue solid line with circle symbols) is calculated from R_0^{tot} ($R_0^{\text{tot},s}$). When the electron concentration of the parallel conduction channel n_p is not extremely large (nearly double the density in the QW), the Eq. (5) is a good approximation.

IV. ILLUMINATION EFFECTS

The relationship between the sheet carrier density and the illumination time t_{LED} is characterized firstly. According to the basic principle of light-matter interaction, n_{QW} and n_p should follow exponential changes during the illumination, i.e., $n_{\text{QW}}(t_{\text{LED}}) = n_{\text{QW},0} + \Delta n_{\text{QW}}\left(1 - e^{-\kappa_{\text{QW}}t_{\text{LED}}}\right)$ and $n_p(t_{\text{LED}}) = n_{p,0} + \Delta n_p\left(1 - e^{-\kappa_p t_{\text{LED}}}\right)$. Here, $n_{\text{QW},0}$ and $n_{p,0}$ are the original sheet electron concentration in the QW and the parallel channels, respectively. Δn_{QW} and Δn_p are their corresponding changes caused by the additional electrons released from DX centers. κ_{QW} and κ_p are relaxation rates. After each illumination for a certain time, a magneto-transport measurement (at 1.7 K) is performed. During the illumination, DX centers become the shallow donor states, described by $DX^- \rightarrow d^0 + e^-$. Furthermore, the d^0 state releases another free electron and becomes the d^+ state [6], as $d^0 \rightarrow d^+ + e^-$. Some of the released electrons stay in the SPSLs, while others will transfer into the QW. As we demonstrate in the following, we find the relationship $\kappa_{\text{QW}} \approx \kappa_p$ holds, allowing us to use a common parameter κ.

The carrier density in the QW can be directly obtained from the SdH oscillation, i.e., $n_{\text{QW}} = n_{\text{SdH}}$. Based on the discussion above, the measured sheet carrier density from the Hall effect becomes

$$n_{\text{Hall}}(t) = n_{\text{Hall},0} + \Delta n_{\text{Hall}}\left(1 - e^{-\kappa t_{\text{LED}}}\right), \tag{6}$$

in which $n_{\text{Hall},0} = n_{\text{QW},0} + 2\alpha_\mu n_{p,0}$ and $\Delta n_{\text{Hall}} = \Delta n_{\text{QW}} + 2\alpha_\mu\Delta n_p$. This formula means that n_{Hall} also follows an exponential change. As shown in Fig. 3(a), the least-squares fittings of n_{SdH} and n_{Hall} are represented by the red dashed line and the blue solid line, respectively. The fitting values of these parameters are $n_{\text{SdH},0} = 1.18 \times 10^{12}$ cm^{-2}, $\Delta n_{\text{SdH}} = 6.95 \times 10^{10}$ cm^{-2}, and $\kappa_{\text{SdH}} = 8.05 \times 10^{-4}$ s^{-1}, while $n_{\text{Hall},0} = 1.20 \times 10^{12}$ cm^{-2}, $\Delta n_{\text{Hall}} = 2.12 \times 10^{11}$ cm^{-2}, and $\kappa_{\text{Hall}} = 7.88 \times 10^{-4}$ s^{-1}. It can be clearly seen that the persistent increase of n_{QW} is only 5.9%. This means that n_{QW} in this SPSL-doped heterostructure is almost stable under illumination. The small increase of the carrier density should be applicable to the lower doping systems due to the special structure of this SPSL doping. Although it is hard to know
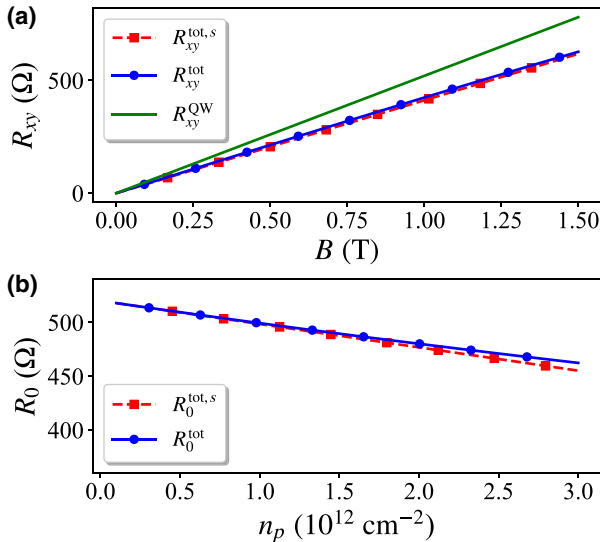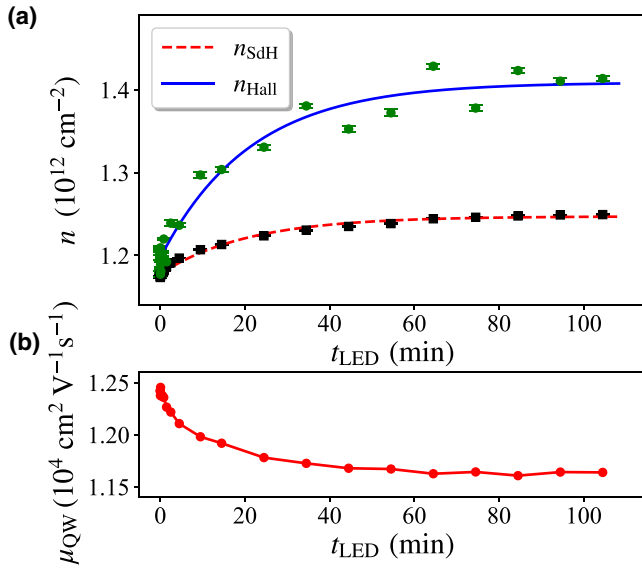
FIG. 3. (a) Sheet carrier density obtained from the Hall effect (green dots) and SdH oscillation (black dots) versus LED illumination time. The blue solid line and the red dashed line are fitting curves. (b) Changes of mobility μ_{QW} after removing the transport contribution from parallel conduction channels. The data are measured at the temperature of 1.7 K.

FIG. 4. SdH oscillation with different illumination time t_{LED}. The black solid line, red dashed line, and blue dotted lines represent the situation of t_{LED} (n_{QW}) as 3.33×10^{-3} min (1.17×10^{12} cm^{-2}), 9.49 min (1.21×10^{12} cm^{-2}), and 1.04×10^2 min (1.25×10^{12} cm^{-2}), respectively. The insert shows their FFTs, which are done using the data from 0.8 T and 4.0 T to reduce the component of zero frequency. Note that the red and blue curves have vertical offset of 0.2 kΩ for clarity. The data are measured at the temperature of 1.7 K.

the absolute value of n_p and μ_p from the Hall resistance R_{xy}, the transport contribution $n_p \mu_p$ can be easily obtained from Eqs. (4)–(6). Note that α_μ may be a time-dependent parameter, while it is regarded as a constant because of the approximately same value of κ_{SdH} and κ_{Hall}.

Figure 4 demonstrates the SdH oscillations after different LED illumination durations (measured at 1.7 K). The clear oscillations can only be seen from 1.5 T due to the high electron density and the relatively low mobility. We also note that the longitudinal resistance R_{xx} keeps unchanged when the magnetic field is smaller than 1 T. Meanwhile, R_0^{QW} is less than 6.5% of R_0^p (zero magnetic longitudinal resistance of parallel channels). They all mean that the contribution from parallel channels to R_{xx} is very small. This can also be verified from the fast Fourier transform (FFT), which has only one peak, as shown in the insert of Fig. 4.

Next, we investigate the effect of illumination on the mobility μ_{QW} and the quantum lifetime $\tau_{q,QW}$. For this, we first calculate the value of $n_p \alpha_\mu$ from $n_{SdH}(t_{LED})$ and $n_{Hall}(t_{LED})$. Then, R_0^{QW} can be extracted from Eq. (5) to remove the transport contribution of the parallel conduction channels. The change of the mobility μ_{QW} is shown in Fig. 3(b), which exhibits a monotone decrease. This is different from the previous result of the modulation-doped GaAs/(Al,Ga)As heterojunction, whose mobility always increases [25]. This heterostructure is heavily doped, and its mobility is lower than conventional heterostructure used for quantum transport and quantum information
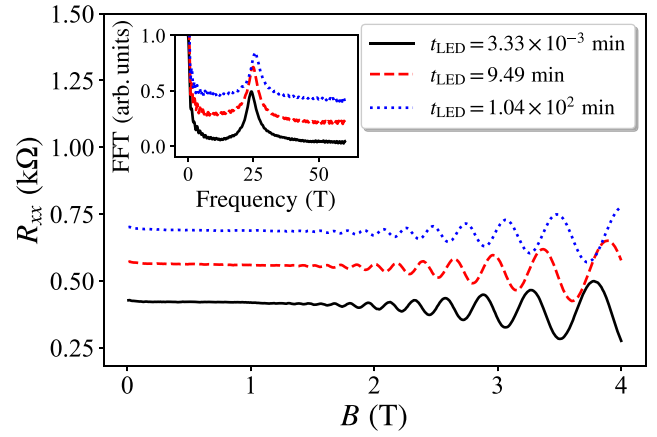
processing. Meanwhile, the Al$_{0.33}$Ga$_{0.67}$As barrier layer between the SPSLs and the QW is only 23 nm, so the scattering of electrons from the ionized donors is very strong. As a consequence of the small QW width, the electron wave function penetrates into the surrounding AlAs layers [26,27], increasing the scattering from interface roughness. According to our estimation, the electron-electron scattering is very small [28–30], which is neglected here.

The quantum lifetime $\tau_{q,QW}$ as a function of illumination time t_{LED} is demonstrated in Fig. 5(a). Its value is obtained by fitting the formula [11,31]

$$\Delta R_{SdH} = 4 R_0^{QW} \exp\left(-\frac{\pi}{\omega_c \tau_{q,QW}}\right) \chi(T), \qquad (7)$$

where ΔR_{SdH} is the SdH oscillation amplitude and $\chi(T) = \beta / \sinh \beta$ with $\beta = 2\pi^2 k_B T / (\hbar \omega_c)$. ω_c is the cyclotron frequency. The so-called Dingle plot is applied to obtain $\tau_{q,QW}$ in Fig. 5(c). After turning on the LED, $\tau_{q,QW}$ becomes slightly longer, then it exhibits an exponential decay until saturation [Fig. 5(a)]. As shown in Fig. 1(b), each DX center releases two electrons after illumination, i.e., $DX^- \rightarrow d^+ + 2e^-$. Most of the excess electrons stay in the SPSLs, enhancing the screening effects. On the other hand, more ionized donors (d^+ states) evolved from DX centers lead to larger potential fluctuations as well as stronger scatterings. The change of $\tau_{q,QW}$ is only 5.1%, which means the scattering of electron keeps nearly a constant after illumination. Therefore, this heterostructure should be very useful for the experiments where the light or photons excite or create
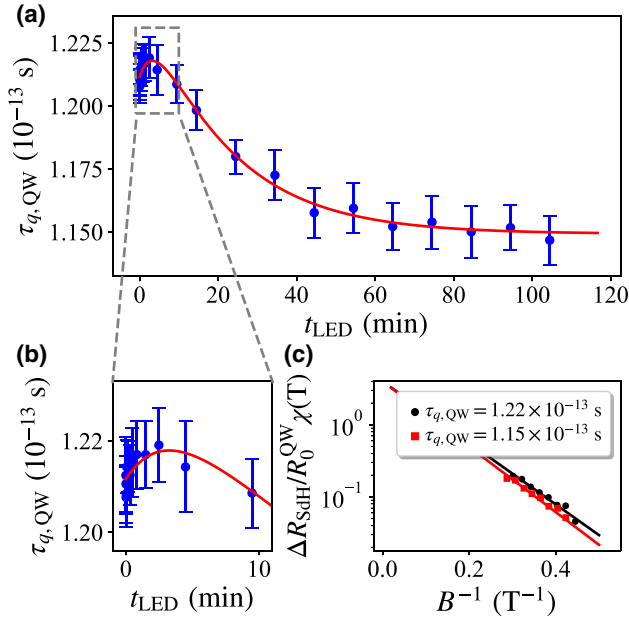
FIG. 5. (a) Quantum lifetime $\tau_{q,\mathrm{QW}}$ versus LED illumination time. The red solid line is the fitting result as described in the main text. (b) The enlarged picture of (a) during t_{LED} about 0–10 min. (c) The Dingle plot of two different $\tau_{q,\mathrm{QW}}$. The circle and square dots are experimental data, while solid curves are fitting results.

specific quantum states without collapsing quantum transport, for example, quantum state conversion from photon polarization to electron spin.

The SPSL-doped GaAs/(Al,Ga)As heterostructure with lower n_{QW} than that used in this paper holds the record high mobility [3], which is due to the excess electron screening (EES) effect. The EES effect is determined by the donor filling fraction f [9,10], whose expression is $n_p = f n_{\mathrm{Si}}$. For this heavily doped heterostructure, the quantum lifetime of the 2DEG in the QW follows

$$\frac{1}{\tau_{q,\mathrm{QW}}} = \frac{1}{\tau_{q,\mathrm{R1}}} + \frac{1}{\tau_{q,\mathrm{R2}}} + \frac{1}{\tau_{q,\mathrm{R3}}} + \frac{1}{\tau_{q,\mathrm{B}}} + \frac{1}{\tau_{q,\mathrm{I}}}. \quad (8)$$

Here, $\tau_{q,\mathrm{B}}$ and $\tau_{q,\mathrm{I}}$ are determined by background impurities and the GaAs/(Al,Ga)As interface roughness [32], respectively. $\tau_{q,\mathrm{R3}}$ is determined by the positively charged donors in the $\mathrm{Al_{0.33}Ga_{0.67}As}$ barrier layers. Since the scatterings of electrons are mainly caused by the Si donors in this heavily doped heterostructure, these three terms are all considered as illumination independent to simplify the following analyses. $\tau_{q,\mathrm{R1}}$ and $\tau_{q,\mathrm{R2}}$ depend on DX centers in this heterostructure and the positively charged donors in the SPSLs, respectively. In the following discussions, $\tau_{q,\mathrm{R2}}$ uses the expression $\tau_{q,\mathrm{R2}} = F_q(f) m_e k_F d_w^3/\hbar$, in which $k_F = \sqrt{2\pi n_{\mathrm{QW}}}$ is the Fermi wave number, m_e is effective electron mass, and d_w is the distance from the doping layers to the center of the QW [9,10]. The factor

$F_q(f)$, as a monotone increasing function of f, accounts for the EES effect. During illumination, the change of $\tau_{q,\mathrm{R1}}^{-1}$ is proportional to the amount of DX centers, i.e., $\Delta\tau_{q,\mathrm{R1}}^{-1} \propto n_{DX}(t) \propto 1 - e^{-\kappa t}$. Note that the sample of this paper is heavily doped, the amount of DX centers should be larger than that of the conventional doping situation.

The red line shown in Fig. 5(a) represents the fitting result. According to the theory [9], we assume $\log F_q(f) = 3.6f - 1.1$, in which $f = f_0 + \Delta f$. f_0 is the initial donors filling fraction. The increase of the filling fraction Δf is $(\Delta n_{\mathrm{Hall}} - \Delta n_{\mathrm{SdH}})/(2\alpha_\mu n_{\mathrm{Si}})$. $\Delta\tau_{q,\mathrm{R1}}^{-1}$ uses the expression $k_{DX}(1 - e^{-\kappa t})$. Other remaining terms in Eq. (8) are rewritten as $\tau_{q,\mathrm{const}}^{-1}$. The fitting values are $f_0 = 25.1\%$, $\alpha_\mu = 3.66 \times 10^{-2}$, $k_{DX}^{-1} = 1.26 \times 10^{-12}$ s, and $\tau_{q,\mathrm{const}} = 1.27 \times 10^{-13}$ s. We also find that the initial filling fraction f_0 calculated by the formula $(n_{\mathrm{Hall,0}} - n_{\mathrm{SdH,0}})/(2\alpha_\mu n_{\mathrm{Si}})$ is only about 6.6%, which is different from the fitting value of 25.1%. One reason is that the screening effect of negatively charged DX centers is taken into consideration for the fitting value 25.1%. Another reason is that the expression of $\tau_{q,\mathrm{R2}}$ considers only the positively charged donors in the GaAs layers of the SPSLs. However, the donors also exist in the AlAs layers of the SPSLs. In the above discussion, we assume that the decay of $\tau_{q,\mathrm{QW}}$ is caused by the conversion of charged impurities from DX centers to d^+ states. This heterostructure is heavily doped and the density of DX centers is very high, the corresponding screening effect cannot be neglected [33–35]. The illumination will destroy the initial correlation between DX centers and d^+ states, increasing the scattering of electrons. Meanwhile, DX centers are strongly localized defects and lie deep in the band gap. DX centers induced potential fluctuations should be smaller compared with d^+ states. Another explanation that may cause the decrease of the $\tau_{q,\mathrm{QW}}$ is the transfer of excess electrons during the illumination. Since the donors tend to migrate along the MBE growth direction [36], the amount of DX centers in the upper AlAs layer of the SPSL is larger than the lower AlAs layer, as shown in Fig. 1(b). After illumination, the upper AlAs layer contains more positively charged donors and attracts more excess electrons from the lower AlAs layer. This would increase the scattering from the SPSL that is close to the surface, while decrease the scattering from another SPSL. Considering the asymmetric wave function of the electrons in the QW and the inhomogeneous illumination from up to down, the final result would be the decay of $\tau_{q,\mathrm{QW}}$.

V. CONCLUSIONS

In conclusion, we investigate the effects of illumination on the heavily doped GaAs/(Al,Ga)As heterostructure with SPSL doping. The increase of the 2DEG concentration of the QW is only 5.9%. Based on the simplified two-band model, the transport contributions from two parallel

SPSLs are removed. Furthermore, we find that the quantum lifetime $\tau_{q,\mathrm{QW}}$ increases firstly and then exhibits an exponential decay after starting of the LED illumination. The increase is due to a larger filling-fraction-enhanced screening effect. The exponential decay may originate from the scattering of the ionized donors d^+ states, which are evolved from DX centers by releasing two electrons. The transfer of excess electrons between the AlAs layers may also cause the decay of $\tau_{q,\mathrm{QW}}$. This work is very useful to understand the mechanism of DX centers for the quantum transport properties of SPSL-doped heterostructures and can also enlarge our scientific knowledge on heavily doped devices. We also note that the SPSL-doped heterostructure is very suitable to study the properties of gate-defined quantum structures formed in ultrahigh mobility 2DEG systems with light illumination, like gate-defined quantum dots for photon-spin state transfer [16–18]. Compared with the conventional layer structure, the small increase of the 2DEG density in the QW can make these kinds of quantum devices more stable during illumination.

[1] K. v. Klitzing, G. Dorda, and M. Pepper, New Method for High-Accuracy Determination of the Fine-Structure Constant Based on Quantized Hall Resistance, Phys. Rev. Lett. **45,** 494 (1980).

[2] H. L. Stormer, D. C. Tsui, and A. C. Gossard, The fractional quantum Hall effect, Rev. Mod. Phys. **71,** S298 (1999).

[3] Y. J. Chung, K. A. V. Rosales, K. W. Baldwin, P. T. Madathil, K. W. West, M. Shayegan, and L. N. Pfeiffer, Ultra-high-quality two-dimensional electron systems, Nat. Mater. **20,** 632 (2021).

[4] Y. J. Chung, K. A. V. Rosales, K. W. Baldwin, K. W. West, M. Shayegan, and L. N. Pfeiffer, Working principles of doping-well structures for high-mobility two-dimensional electron systems, Phys. Rev. Mater. **4,** 044003 (2020).

[5] M. J. Manfra, Molecular beam epitaxy of ultra-high-quality AlGaAs/GaAs heterostructures: Enabling physics in low-dimensional electronic systems, Annu. Rev. Condens. Matter Phys. **5,** 347 (2014).

[6] D. J. Chadi and K. J. Chang, Energetics of DX-center formation in GaAs and $Al_x Ga_{1-x}As$ alloys, Phys. Rev. B **39,** 10063 (1989).

[7] T. Fujita, R. Hayashi, M. Kohda, J. Ritzmann, A. Ludwig, J. Nitta, A. D. Wieck, and A. Oiwa, Distinguishing persistent effects in an undoped GaAs/AlGaAs quantum well by top-gate-dependent illumination, J. Appl. Phys. **129,** 234301 (2021).

[8] V. Umansky, M. Heiblum, Y. Levinson, J. Smet, J. Nübler, and M. Dolev, MBE growth of ultra-low disorder 2DEG with mobility exceeding 35×10^6 cm^2/Vs, J. Cryst. Growth **311,** 1658 (2009).

[9] M. Sammon, T. Chen, and B. I. Shklovskii, Excess electron screening of remote donors and mobility in modern GaAs/AlGaAs heterostructures, Phys. Rev. Mater. **2,** 104001 (2018).

[10] M. Sammon, M. A. Zudov, and B. I. Shklovskii, Mobility and quantum mobility of modern GaAs/AlGaAs heterostructures, Phys. Rev. Mater. **2,** 064604 (2018).

[11] T. Akiho and K. Muraki, Screening Effects of Superlattice Doping on the Mobility of GaAs Two-Dimensional Electron System Revealed by in situ Gate Control, Phys. Rev. Appl. **15,** 024003 (2021).

[12] C. Rössler, T. Feil, P. Mensch, T. Ihn, K. Ensslin, D. Schuh, and W. Wegscheider, Gating of high-mobility two-dimensional electron gases in GaAs/AlGaAs heterostructures, New J. of Phys. **12,** 043007 (2010).

[13] K.-J. Friedland, R. Hey, H. Kostial, R. Klann, and K. Ploog, New Concept for the Reduction of Impurity Scattering in Remotely Doped GaAs Quantum Wells, Phys. Rev. Lett. **77,** 4616 (1996).

[14] S. Ji, T. Tajiri, H. Kiyama, A. Oiwa, and S. Iwamoto, Design of bull's-eye optical cavity toward efficient quantum media conversion using gate-defined quantum dot, Jpn. J. Appl. Phys. **60,** 102003 (2021).

[15] T. Tajiri, Y. Sakai, K. Kuruma, S. M. Ji, H. Kiyama, A. Oiwa, J. Ritzmann, A. Ludwig, A. D. Wieck, Y. Ota, Y. Arakawa, and S. Iwamoto, Fabrication and optical characterization of photonic crystal nanocavities with electrodes for gate-defined quantum dots, Jpn. J. Appl. Phys. **59,** SGGI05 (2020).

[16] R. Vrijen and E. Yablonovitch, A spin-coherent semiconductor photo-detector for quantum communication, Physica E **10,** 569 (2001).

[17] T. Fujita, K. Morimoto, H. Kiyama, G. Allison, M. Larsson, A. Ludwig, S. R. Valentin, A. D. Wieck, A. Oiwa, and S. Tarucha, Angular momentum transfer from photon polarization to an electron spin in a gate-defined quantum dot, Nat. Commun. **10,** 2991 (2019).

[18] K. Kuroyama, M. Larsson, C. Y. Chang, J. Muramoto, K. Heya, T. Fujita, G. Allison, S. R. Valentin, A. Ludwig, A. D. Wieck, S. Matsuo, A. Oiwa, and S. Tarucha, Photogeneration of a single electron from a single zeeman-resolved light-hole exciton with preserved angular momentum, Phys. Rev. B **99,** 085203 (2019).

[19] S. Yamada, K. Maezawa, W. T. Yuen, and R. A. Stradling, X-conduction-electron transport in very thin AlAs quantum wells, Phys. Rev. B **49,** 2189 (1994).

[20] K. Vakili, Y. P. Shkolnikov, E. Tutuc, E. P. De Poortere, and M. Shayegan, Spin Susceptibility of Two-Dimensional

Electrons in Narrow AlAs Quantum Wells, Phys. Rev. Lett. **92,** 226401 (2004).

[21] H. Momose, N. Mori, C. Hamaguchi, T. Ikaida, H. Arimoto, and N. Miura, Cyclotron resonance in $(GaAs)_n/(AlAs)_n$ superlattices under ultra-high magnetic fields, Physica E **4,** 286 (1999).

[22] S. Peters, L. Tiemann, C. Reichl, S. Fält, W. Dietsche, and W. Wegscheider, Improvement of the transport properties of a high-mobility electron system by intentional parallel conduction, Appl. Phys. Lett. **110,** 042106 (2017).

[23] J. J. Harris, Simplified assessment of parallel conduction in modulation-doped heterostructures, Meas. Sci. Technol. **2,** 1201 (1991).

[24] M. J. Kane, N. Apsley, D. A. Anderson, L. L. Taylor, and T. Kerr, Parallel conduction in $GaAs/Al_xGa_{1-x}As$ modulation doped heterojunctions, J. Phys. C: Solid State Phys. **18,** 5629 (1985).

[25] M. Hayne, A. Usher, J. J. Harris, V. V. Moshchalkov, and C. T. Foxon, Remote impurity scattering in modulation-doped $GaAs/Al_xGa_{1-x}As$ heterojunctions, Phys. Rev. B **57,** 14813 (1998).

[26] H. Sakaki, T. Noda, K. Hirakawa, M. Tanaka, and T. Matsusue, Interface roughness scattering in GaAs/AlAs quantum wells, Appl. Phys. Lett. **51,** 1934 (1987).

[27] A. Gold, Electronic transport properties of a two-dimensional electron gas in a silicon quantum-well structure at low temperature, Phys. Rev. B **35,** 723 (1987).

[28] X. Fu, A. Riedl, M. Borisov, M. A. Zudov, J. D. Watson, G. Gardner, M. J. Manfra, K. W. Baldwin, L. N. Pfeiffer, and K. W. West, Effect of illumination on quantum lifetime in GaAs quantum wells, Phys. Rev. B **98,** 195403 (2018).

[29] G. F. Giuliani and J. J. Quinn, Lifetime of a quasiparticle in a two-dimensional electron gas, Phys. Rev. B **26,** 4421 (1982).

[30] I. A. Dmitriev, M. G. Vavilov, I. L. Aleiner, A. D. Mirlin, and D. G. Polyakov, Theory of microwave-induced oscillations in the magnetoconductivity of a two-dimensional electron gas, Phys. Rev. B **71,** 115316 (2005).

[31] P. T. Coleridge, Small-angle scattering in two-dimensional electron gases, Phys. Rev. B **44,** 3793 (1991).

[32] A. Gold, Scattering time and single-particle relaxation time in a disordered two-dimensional electron gas, Phys. Rev. B **38,** 10798 (1988).

[33] Z. Wilamowski, J. Kossut, T. Suski, P. Wisniewski, and L. Dmowski, Appearance and destruction of spatial correlation of DX charges in GaAs, Semicond. Sci. Technol. **6,** B34 (1991).

[34] Z. Wilamowski, J. Kossut, W. Jantsch, and G. Ostermayer, DX centres and Coulomb potential fluctuations, Semicond. Sci. Technol. **6,** B38 (1991).

[35] D. M. Larsen, Screening by fixed charges in compensated semiconductors, Phys. Rev. B **11,** 3904 (1975).

[36] L. Pfeiffer, E. F. Schubert, K. W. West, and C. W. Magee, Si dopant migration and the AlGaAs/GaAs inverted interface, Appl. Phys. Lett. **58,** 2258 (1991).